Alma Mater Studiorum Università di Bologna
Archivio istituzionale della ricerca

Zirconium metal−organic frameworks containing a biselenophene linker: Synthesis, characterization, and luminescent properties

(Article begins on next page)

26 June 2024

Zirconium Metal-Organic Frameworks containing a biselenophene linker: synthesis, characterization and luminescent properties

Journal:	*Inorganic Chemistry*
Manuscript ID	Draft
Manuscript Type:	Article
Date Submitted by the Author:	n/a
Complete List of Authors:	Mercuri, Giorgio; Istituto di Chimica dei Composti Organo Metallici Consiglio Nazionale Delle Ricerche Sezione di Firenze Moroni, Marco; Università degli Studi dell'Insubria Dipartimento di Scienza e Alta Tecnologia Fermi, Andrea; Alma Mater Studiorum Università di Bologna, Dipartimento di Chimica "Giacomo Ciamician" Bergamini, Giacomo; Universita degli Studi di Bologna, Chemistry Ciamician Galli, Simona; Universita dell'Insubria Dipartimento di Diritto Economia e Culture, Dipartimento di Scienza e Alta Tecnologia Giambastiani, Giuliano; National Research Council, Institute of Chemistry of OrganoMetallic Compounds Rossin, Andrea; Istituto di Chimica dei Composti Organo Metallici Consiglio Nazionale Delle Ricerche Sezione di Firenze,

SCHOLARONE™
Manuscripts

1
2
3
4
5
6
7
8
9
10
11
12
13
14
15
16
17
18
19
20
21
22
23
24
25
26
27
28
29
30
31
32
33
34
35
36
37
38
39
40
41
42
43
44
45
46
47
48
49
50
51
52
53
54
55
56
57
58
59
60

Zirconium Metal-Organic Frameworks containing a biselenophene linker: synthesis, characterization and luminescent properties

Giorgio Mercuri,[a,b] Marco Moroni,[c] Andrea Fermi,[d,]* Giacomo Bergamini,[d] Simona Galli,[c,]*

Giuliano Giambastiani,[a,e,f] and Andrea Rossin [a,]*

[a] Istituto di Chimica dei Composti Organometallici (ICCOM-CNR),
Via Madonna del Piano 10, 50019 Sesto Fiorentino, Italy.

[b] Scuola di Scienze e Tecnologie, Università di Camerino,
Via S. Agostino 1, 62032 Camerino, Italy.

[c] Dipartimento di Scienza e Alta Tecnologia, Università dell'Insubria,
Via Valleggio 11, 22100 Como, Italy.

[d] Dipartimento di Chimica "G. Ciamician", Università di Bologna,
Via Selmi 2, 40126 Bologna, Italy.

[e] Institute of Chemistry and Processes for Energy, Environment and Health (ICPEES), UMR 7515
CNRS-University of Strasbourg (UdS), 25, rue Becquerel, 67087 Strasbourg Cedex 02, France.

[f] Kazan Federal University, Alexander Butlerov Institute of Chemistry,
420008 Kazan, Russian Federation.

Authors to whom correspondence should be addressed: a.rossin@iccom.cnr.it;
simona.galli@uninsubria.it; andrea.fermi2@unibo.it.

Abstract. The bicyclic ditopic linker 2,2'-biselenophene-5,5'-dicarboxylic acid (**H₂SpSp**) specifically designed for MOFs construction has been synthesized in good yields and fully characterized. The corresponding zirconium MOF $[Zr_6O_4(OH)_4(SpSp)_{3.8}Cl_{4.4}]$ (**1**) (where missing linkers are replaced by chloride anions as shown by XRF and elemental analysis) is isostructural with its bithiophene and bithiazole analogues. Starting from **1**, an extension of the biselenophene-based zirconium MOFs family has been successfully achieved exploiting the structural analogy of the five-membered heterocycles selenophene, thiophene and thiazole. Thus, three mixed-linker MOFs containing variable amounts of different bis(heterocyclic) dicarboxylic acids have been prepared and fully characterized: the two double-mixed $[Zr_6O_4(OH)_4(SpSp)_{2.6}(ThTh)_{1.3}Cl_{4.2}]$ (**2; H₂ThTh** = 2,2'-bithiophene-5,5'-dicarboxylic acid) and $[Zr_6O_4(OH)_4(SpSp)_2(TzTz)_{1.8}Cl_{4.4}]$ (**3; H₂TzTz** = 2,2'-bithiazole-5,5'-dicarboxylic acid) materials, as well as the triple-mixed $[Zr_6O_4(OH)_4(SpSp)_{1.6}(ThTh)_{1.2}(TzTz)_{1.4}Cl_{3.6}]$ (**4**) compound. The four MOFs are luminescent under UV irradiation, exhibiting emission wavelengths falling in the blue-green visible region, as observed for their constitutive linkers. These materials open new horizons in the preparation of porous luminescent sensors or multicolor emitters for LEDs.

Introduction

The design, synthesis and characterization of Metal-Organic Frameworks (MOFs) for assorted applications is nowadays one of the most fruitful research fields in inorganic chemistry and materials science.[1] The extreme versatility in MOFs design, obtained through a judicious combination of metallic nodes and organic linkers, and their high crystallinity degree are key features that can be exploited in a plethora of applicative fields. While MOFs featuring fully carbocyclic or nitrogen-containing heterocyclic spacers are ubiquitous, much fewer examples are found with sulphur- or selenium-based heterocycles like thiophene, thiazole and selenophene. The latter in particular has been very little explored as organic building block for MOFs construction. To date, the only literature examples are limited to the simple selenophene-2,5-dicarboxylic acid in combination with Zn^{II} and Cd^{II}, as reported by the group of D'Alessandro and co-workers.[2] Fully organic selenophene-based polymers are attracting much attention in materials science for their potential technological applications in light-emitting diodes (LEDs), organic solar cells and other electronic components, since they have appropriate absorption and emission band ranges and suitable HOMO-LUMO energy levels.[3] Given the peculiar luminescence properties of selenophene, it would be desirable to incorporate it into tailor-made linkers for MOFs construction. Inspired by this idea and following our recent preparation of a bithiazole linker and the related zirconium MOF,[4] in this work we describe the preparation of the new 2,2'-biselenophene-5,5'-dicarboxylic acid (**H₂SpSp**, Scheme 1). Successively, we tested its coordination ability towards zirconium: combination with Zr^{IV} sources under solvothermal conditions has led to the obtainment of the related MOF of general formula $[Zr_6O_4(OH)_4(SpSp)_{3.8}Cl_{4.4}]$ (**1**, Figure 1) sharing the same structural motif of UiO-67[5] and isostructural with the already known bithiophene[6] and bithiazole[4] analogues. **1** has been fully characterized in the solid state. In the MOFs world, the introduction of chemically different but structurally similar linkers within the same MOF crystal structure leads to the so-called mixed Metal-Organic Frameworks [MIXMOFs or Multivariate (MTV)-MOFs].[7] MIXMOFs grant pore walls heterogeneity, preserving at the same time the structural motif of the parent single-linker homologue.

Aiming at extending the biselenophene-based MOF family (and given the structural analogy between biselenophene, bithiophene and bithiazole), we have also synthesized three Zr^{IV} MIXMOFs isostructural with **1**: the two double-mixed biselenophene-bithiophene $[Zr_6O_4(OH)_4(SpSp)_{2.6}(ThTh)_{1.3}Cl_{4.2}]$ (**2; H$_2$ThTh** = 2,2'-bithiophene-5,5'-dicarboxylic acid, Scheme 1) and biselenophene-bithiazole $[Zr_6O_4(OH)_4(SpSp)_2(TzTz)_{1.8}Cl_{4.4}]$ (**3; H$_2$TzTz** = 2,2'-bithiazole-5,5'-dicarboxylic acid, Scheme 1) materials, as well as the triple-mixed $[Zr_6O_4(OH)_4(SpSp)_{1.6}(ThTh)_{1.2}(TzTz)_{1.4}Cl_{3.6}]$ (**4**) compound. All the samples are defective; missing linkers are balanced by chloride anions bound to zirconium, as inferred from elemental analysis, XRF spectroscopy and powder X-ray diffraction structure determination. The actual ligand composition within the MIXMOFs has been assessed *via* ^{1}H NMR signal integration after sample digestion in acidic solution. The luminescent properties of **1-4** have been finally investigated and compared. As their constitutive linkers, all (MIX)MOF samples in DMF suspensions are featured by emissions falling in the blue-green visible range (λ_{em} between 450 and 510 nm).
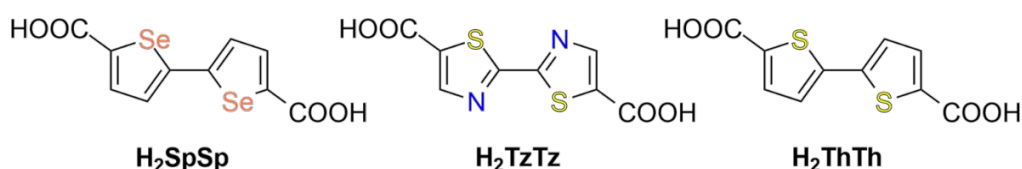
Scheme 1. Molecular structures of the linkers used in this study: 2,2'-biselenophene-5,5'-dicarboxylic acid (**H$_2$SpSp**), 2,2'-bithiazole-5,5'-dicarboxylic acid (**H$_2$TzTz**) and 2,2'-bithiophene-5,5'-dicarboxylic acid (**H$_2$ThTh**).

Experimental Section

Materials and Methods. All the chemicals and reagents employed were purchased from commercial vendors and used as received without further purification. **H$_2$TzTz**,[4] **H$_2$ThTh**[6] and ethyl selenophene-2-carboxylate[8] were prepared according to the published procedures. For the organic syntheses, solvents were purified through standard distillation techniques. Deuterated solvents (Sigma Aldrich) were stored over 4 Å molecular sieves and degassed by three freeze-pump-thaw cycles before use. NMR spectra were recorded on a BRUKER AVANCE 400 MHz

spectrometer. ^{1}H and ^{13}C{^{1}H} NMR chemical shifts are reported in parts per million (ppm) downfield of tetramethylsilane (TMS) and were calibrated against the residual resonance of the protiated part of the deuterated solvent. FT-IR spectra (KBr pellets) were recorded on a Perkin-Elmer Spectrum BX Series FTIR spectrometer, in the 4000−400 cm$^{−1}$ range, with a 2 cm$^{−1}$ resolution. Thermogravimetric analysis (TGA) measurements were performed under N_2 flow (100 mL min^{-1}) at a heating rate of 10 K min^{-1} on an EXSTAR Thermo Gravimetric Analyzer (TG-DTG) Seiko 6200. Differential scanning calorimetry (DSC) measurements were carried out on a NETZSCH STA 409 PC analyzer, heating up ~10 mg powdered samples, placed in alumina crucibles, under a N_2 flow (40 mL min$^{−1}$) from 303 to 1173 K, with a rate of 10 K min^{-1}. Raw DSC data were corrected based on a background curve previously acquired in the same experimental conditions. Elemental analyses were performed at ICCOM-CNR using a Thermo FlashEA 1112 Series CHNS-O elemental analyzer with an accepted tolerance of ± 2%. ESI-MS spectra were recorded by direct introduction of the analyte solution (10 μL/min) on a FinniganLTQ mass spectrometer (Thermo, San Jose, CA). The instrument was equipped with a conventional ESI source. The working conditions were the following: negative polarity, spray voltage 5 kV, capillary voltage −18 V, capillary temperature 563 K and tube lens −87 V. Sheath gas was set at 10 a.u. and auxiliary gas was kept at 3 a.u. For the acquisitions, the Xcalibur 2.0 software (Thermo) was used. Aqueous solutions of **H$_2$SpSp** were prepared using 1 mg/mL and then diluting to 10 ng/μL with 95% v/v water and 5% v/v acetonitrile. Powder X-ray diffraction (PXRD) qualitative measurements were carried out in the 4-50° 2θ region with a Panalytical X'PERT PRO powder diffractometer equipped with a diffracted beam Ni filter, a PIXcel$^©$ solid state detector and a Cu Kα X-ray source (λ = 1.5418 Å). Slits were used on both the incident (Soller slits aperture 0.25°; divergence slit aperture 0.5°) and the diffracted (anti-scatter slit height 7.5 mm) beam. X-ray fluorescence (XRF) analyses were performed on powdered batches (*ca.* 10 mg for each MOF sample) with a Panalytical MINIPAL 2 instrument equipped with a Cr X-ray source.

Synthesis of diethyl [2,2'-biselenophene]-5,5'-dicarboxylate (Et$_2$SpSp). The 2,2′-biselenophene-5,5′-diester was prepared through an Ag^I/Pd^{II}-catalysed homocoupling of ethyl selenophene-2-carboxylate, following the literature procedure found for its thiophene analogue.[9] The full experimental details are reported hereafter, for the sake of completeness. Ethyl selenophene-2-carboxylate (480 mg, 2.36 mmol) was dissolved in freshly distilled dimethyl sulfoxide (DMSO, 14 mL) in a Schlenk round-bottom flask equipped with a magnetic stirring bar. Then, silver fluoride (AgF, 600 mg, 4.72 mmol) and the Pd^{II} catalyst bis(benzonitrile)palladium dichloride [PdCl$_2$(C$_6$H$_5$CN)$_2$, 27.1 mg, 0.07 mmol] were added to this solution while stirring at ambient temperature. Afterwards, the resulting mixture was heated at 333 K for 5 h. Then, it was cooled to room temperature and passed through a Celite pad, which was successively washed with chloroform (3 × 10 mL). The dark yellow organic filtrate was washed with water (3 × 10 mL) and the aqueous layer extracted with chloroform (3 × 10 mL). The combined organic layers were dried over anhydrous sodium sulfate and concentrated under reduced pressure to leave a crude solid that was finally purified through column chromatography on silica gel (eluent: petroleum ether/ethyl acetate 85:15). The dark yellow solid residue obtained after solvent removal was recovered and dried under vacuum. Yield: 405 mg (85%). Single crystals suitable for X-ray diffraction were obtained through ambient temperature slow evaporation of an ethyl acetate concentrated solution. The details of the single-crystal X-ray diffraction data acquisition and treatment as well as the crystal and molecular structure are reported in the Supporting Information (Figure S1 and Table S1).
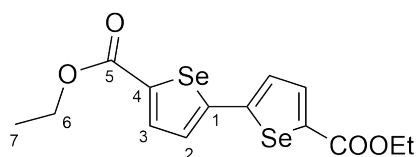
^{1}H NMR (400 MHz, CD$_2$Cl$_2$, 298 K, ppm): δ 1.36 (t, $^3J_{HH}$ = 7.1 Hz, 6H, H^7), 4.31 (q, $^3J_{HH}$ = 7.1 Hz, 4H, H^6), 7.37 (d, $^3J_{HH}$ = 3.9 Hz, 2H, H^3), 7.90 (d, $^3J_{HH}$ = 3.9 Hz, 2H, H^2). ^{13}C{^{1}H} NMR (100 MHz, CD$_2$Cl$_2$, 298 K, ppm): δ 14.1 (C^7), 61.5 (C^6), 128.3 (C^2), 136.2 (C^3), 139.1 (C^1), 150.5 (C^4), 162.9 (C^5). Elem. Anal. Calc. (%) for **Et$_2$SpSp**, C$_{14}$H$_{14}$O$_4$Se$_2$ (FW = 404.18 g/mol): C 41.60, H 3.49;

found C 41.62, H 3.52. IR (KBr pellet, cm^{-1}): ν = 3043 (w), 2988 (w), 2976 (w), 2901 (w), 2867 [w, ν(C–H)], 1685 [s, ν(C=O)], 1525 [m, ν(C=C)], 1442 [s, δ(CH$_2$/CH$_3$)], 1261 [s, δ(O–Et)], 747 [s, γ(C–H)].

Synthesis of 2,2'-biselenophene-5,5'-dicarboxylic acid (H$_2$SpSp). A freshly prepared NaOH 1 M aqueous solution (8.5 mL) was added to a suspension of diethyl [2,2'-biselenophene]-5,5'-dicarboxylate (360 mg, 0.88 mmol) in methanol (8.5 mL), and the resulting mixture was brought to 328 K and kept at this temperature for 2 h. After that time, the clear yellow solution formed was cooled down to ambient temperature. TLC analysis (petroleum ether/ethyl acetate 5:1) showed no more ester starting material. Methanol was removed by rotary evaporation and the residual aqueous phase was acidified with HCl 1 M until very low pH values (3-4). During HCl addition, **H$_2$SpSp** started to precipitate. The reaction flask was left at low temperature (277 K) for some hours in order to facilitate the precipitation. The yellow solid recovery was achieved through filtration on filter paper. Yield: 245 mg (80%).
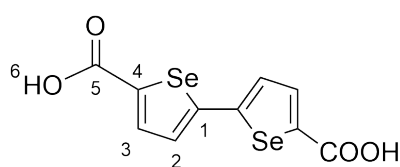
^{1}H NMR (400 MHz, DMSO-d_6, 298 K, ppm): δ 7.57 (d, $^3J_{HH}$ = 4.1 Hz, 2H, H^3), 7.84 (d, $^3J_{HH}$ = 4.1 Hz, 2H, H^2), 13.25 (s, br, 2H, H^6). ^{13}C{^{1}H} NMR (100 MHz, DMSO-d_6, 298 K, ppm): δ 129.4 (C^2), 136.5 (C^3), 140.0 (C^1), 149.6 (C^4), 163.8 (C^5). Elem. Anal. Calc. for **H$_2$SpSp**, C$_{10}$H$_6$O$_4$Se$_2$ (MW = 348.07 g/mol): C, 34.51; H, 1.74. Found: C, 34.53; H, 1.76. ESI-MS/MS: m/z = 347 (M-H)$^-$, m/z = 303 (M-H-CO$_2$)$^-$, m/z = 173 (M-2H)$^{2-}$. IR (KBr pellet, cm^{-1}): ν = 3423 [s, br, ν(O-H)], 3048 [w, ν(C-H)], 1655 [m, ν(C=O)], 1526 [m, ν(C=C)], 1395 [s, δ(CH)], 763 [m, γ(C-H)], 466 [w, ν(C-Se)].

Synthesis of [Zr$_6$O$_4$(OH)$_4$(SpSp)$_{3.8}$Cl$_{4.4}$]·4(DMF)·8(H$_2$O) (1·S).[10] Following the improved preparation of UiO-67 reported by Fahra *et al.*,[11] zirconium chloride [ZrCl$_4$, 67.6 mg, 0.29 mmol] and a concentrated (12 M) HCl aqueous solution (0.5 mL) were mixed together and diluted with *N,N*-dimethylformamide (DMF, 5 mL). The resulting suspension was sonicated in an ultrasonic bath at

ambient temperature for 15 minutes. After that time, the ligand **H₂SpSp** (100 mg, 0.29 mmol) was

added to the clear colorless solution; the mixture was further diluted with fresh DMF (7 mL),

sonicated for additional 15 minutes and finally transferred to a Teflon-lined stainless steel autoclave

(inner Teflon beaker volume ca. 20 mL). The autoclave was sealed and heated at 363 K for 24 h under

autogenous pressure. After slow overnight cooling, a yellow powder of **1·S** formed at the bottom of

the beaker. It was collected, washed with ethanol (4 × 10 mL), petroleum ether (4 × 10 mL) and

finally dried under a nitrogen stream at room temperature. Yield: 109 mg (87% based on zirconium).

The phase purity of every batch was checked through PXRD. Elemental analysis calcd (%) for **1·S**,

$C_{50}H_{63.2}Cl_{4.4}N_4O_{35.2}Se_{7.6}Zr_6$ (MW = 2586.88 g/mol): C 23.10, H 2.44, N 2.16; found: C 23.09, H 2.41,

N 2.12. IR [ν(C=O)] band (KBr, cm⁻¹, Figure S2): 1651 (m).

Synthesis of [Zr₆O₄(OH)₄(SpSp)₂.₆(ThTh)₁.₃Cl₄.₂]·4(DMF)·6(H₂O) (2·S).[10] Zirconium chloride

[ZrCl₄, 70.0 mg, 0.30 mmol] and a concentrated (12 M) HCl aqueous solution (0.5 mL) were mixed

together and diluted with DMF (5 mL). The resulting suspension was sonicated in an ultrasonic bath

at ambient temperature for 15 minutes. After that time, the ligands **H₂SpSp** (52.2 mg, 0.15 mmol)

and **H₂ThTh** (38.1 mg, 0.15 mmol) were added to the clear colorless solution; the mixture was further

diluted with fresh DMF (7 mL), sonicated for additional 15 minutes and finally transferred to a

Teflon-lined stainless steel autoclave (inner Teflon beaker volume ca. 20 mL). The autoclave was

sealed and heated at 363 K for 24 h under autogenous pressure. After slow overnight cooling, a yellow

powder of **2·S** formed at the bottom of the beaker. It was collected, washed with ethanol (4 × 10 mL),

petroleum ether (4 × 10 mL) and finally dried under a nitrogen stream at room temperature. Yield:

110 mg (90% based on zirconium). The phase purity of every batch was checked through PXRD.

Elemental analysis calcd (%) for **2·S**, $C_{51}H_{59.6}Cl_{4.2}N_4O_{33.6}S_{2.6}Se_{5.2}Zr_6$ (MW = 2456.42 g/mol): C

24.91, H 2.44, N 2.28; S, 3.39; found: C 25.05, H 2.46, N 2.31; S, 3.43. IR [ν(C=O)] bands (KBr,

cm⁻¹, Figure S2): 1704, 1662 (m).

Synthesis of [Zr$_6$O$_4$(OH)$_4$(SpSp)$_2$(TzTz)$_{1.8}$Cl$_{4.4}$]·4(DMF)·2(H$_2$O) (3·S).[10] Zirconium chloride [ZrCl$_4$, 70.0 mg, 0.30 mmol] and a concentrated (12 M) HCl aqueous solution (0.5 mL) were mixed together and diluted with DMF (5 mL). The resulting suspension was sonicated in an ultrasonic bath at ambient temperature for 15 minutes. After that time, the ligands **H$_2$SpSp** (52.2 mg, 0.15 mmol) and **H$_2$TzTz** (38.4 mg, 0.15 mmol) were added to the clear colorless solution; the mixture was further diluted with fresh DMF (7 mL), sonicated for additional 15 minutes and finally transferred to a Teflon-lined stainless steel autoclave (inner Teflon beaker volume ca. 20 mL). The autoclave was sealed and heated at 363 K for 24 h under autogenous pressure. After slow overnight cooling, a microcrystalline yellow powder of **3·S** formed at the bottom of the beaker. It was collected, washed with ethanol (4 × 10 mL), petroleum ether (4 × 10 mL) and finally dried under a nitrogen stream at room temperature. Yield: 106 mg (92 % based on zirconium). The phase purity of every batch was checked through PXRD. Elemental analysis calcd (%) for **3·S**, C$_{46.4}$H$_{47.6}$Cl$_{4.4}$N$_{7.6}$O$_{29.2}$S$_{3.6}$Se$_4$Zr$_6$ (MW = 2313.51 g/mol): C 24.07, H 2.07, N 4.60; S, 4.99; found: C 24.29, H 2.06, N 4.62; S, 4.97. IR [ν(C=O)] bands (KBr, cm^{-1}, Figure S2): 1654, 1580 (m).

Synthesis of [Zr$_6$O$_4$(OH)$_4$(SpSp)$_{1.6}$(ThTh)$_{1.2}$(TzTz)$_{1.4}$Cl$_{3.6}$]·5(DMF)·12(H$_2$O) (4·S).[10] Zirconium oxychloride octahydrate [ZrOCl$_2$·8H$_2$O, 96.7 mg, 0.30 mmol] and a concentrated (12 M) HCl aqueous solution (0.5 mL) were mixed together and diluted with DMF (5 mL). The resulting suspension was sonicated in an ultrasonic bath at ambient temperature for 15 minutes. After that time, the ligands **H$_2$SpSp** (34.8 mg, 0.10 mmol), **H$_2$TzTz** (25.6 mg, 0.10 mmol) and **H$_2$ThTh** (25.4 mg, 0.10 mmol) were added to the clear colorless solution; the mixture was further diluted with fresh DMF (7 mL), sonicated for additional 15 minutes and finally transferred to a Teflon-lined stainless steel autoclave (inner Teflon beaker volume ca. 20 mL). The autoclave was sealed and heated at 363 K for 24 h under autogenous pressure. After slow overnight cooling, a yellow powder of **4·S** formed at the bottom of the beaker. It was collected, washed with ethanol (4 × 10 mL), petroleum ether (4 × 10 mL) and finally dried under a nitrogen stream at room temperature. Yield: 110 mg (85% based on

zirconium). The phase purity of each batch was checked through PXRD. Elemental analysis calcd (%) for **4·S**, $C_{54.2}H_{77}Cl_{3.6}N_{7.8}O_{41.8}S_{5.2}Se_{3.2}Zr_6$ (MW = 2600.99 g/mol): C 25.00, H 2.98, N 4.20; S, 6.41; found: C 25.43, H 3.01, N 4.28; S, 6.38. IR [ν(C=O)] bands (KBr, cm^{-1}, Figure S2): 1658, 1590, 1520 (s).

Powder X-ray Diffraction Structure Determination. Powdered samples (~50 mg) of **1·S-4·S** were deposited in the cavity of a silicon free-background sample-holder 0.2 mm deep (Assing Srl, Monterotondo, Italy). Powder X-ray diffraction (PXRD) data acquisitions were carried out with a Bruker AXS D8 Advance vertical-scan θ:θ diffractometer, equipped with an X-ray tube (Cu Kα, λ = 1.5418 Å), a Bruker Lynxeye linear position-sensitive detector, a filter of nickel in the diffracted beam and the following optical components: primary beam Soller slits (2.5°), fixed divergence slit (0.5°), antiscatter slit (8 mm). The generator was set at 40 kV and 40 mA. Preliminary PXRD analyses to unveil the purity and crystallinity of the samples were performed in the 2θ range 3.0-35.0°, with steps of 0.02° and time *per* step of 1 s. PXRD acquisitions for the assessment of the crystal structure were performed overnight with steps of 0.02° and in the 2θ range reported in Table 1.

Table 1. Experimental conditions of the PXRD data acquisitions carried out on **1·S-4·S**.

	1·S	**2·S**	**3·S**	**4·S**
2θ range (°)	3.0-105.0	4.5-105.0	5.0-105.0	4.5-105.0

A visual comparison between the PXRD patterns of the MOFs under study with those of the $[Zr_6O_4(OH)_4(L)_6]\cdot n(DMF)$ analogues (L = ThTh^{2-} = [2,2′-bithiophene]-5,5′-dicarboxylate;[6] L = TzTz^{2-} = [2,2′-bithiazole]-5,5′-dicarboxylate[4]) highlighted that the compounds are isostructural. This suggestion was confirmed by performing a whole powder pattern refinement with the Le Bail approach as implemented in TOPAS-R V3,[12] starting from the unit cell parameters of the parent

bithiophene MOF. The crystallographically independent portion of the ligand and the DMF molecules were described using rigid bodies built up through the z-matrix formalism. In the case of **2·S-4·S**, the co-presence of the $SpSp^{2-}$, $ThTh^{2-}$ and $TzTz^{2-}$ ligands was taken into account by including into the structural model the rigid body of $SpSp^{2-}$ and inserting proper vicariant atoms (S *vs*. Se for $ThTh^{2-}$; S *vs*. Se and N *vs*. CH for $TzTz^{2-}$) setting their molar ratios at the values obtained from the ^{1}H-NMR signal integration of the digested samples (see the Supporting Information). In the initial steps of the structure determination, both the metal cluster components (i.e. Zr^{4+}, O^{2-} and OH^-) and the spacers were positioned according to the crystal structure of $[Zr_6O_4(OH)_4(ThTh)_6]\cdot n(DMF)$. Average values were assigned to bond distances and angles.[13] When allowed by the symmetry, the position and orientation of the independent components of the MOFs were let vary. To account for the possibility of missing-ligand defects, a known phenomenon for UiO-type materials,[14] the linkers site occupation factors were refined, reaching in all compounds a value lower than one. As assessed by X-ray fluorescence (Figures S3-S6), the missing negative charges are compensated by chloride anions. On the basis of a search in the Cambridge Structural Database (v. 2020.1) for Zr_6Cl_x clusters (no $Zr_6Cl_xO_y$ clusters were found), it was assumed that the chloride anions in **1·S-4·S** are bound to the Zr^{IV} cations as terminal ligands vicariant to the oxygen atoms of the carboxylate groups. They were placed accordingly in all the positions where their site occupation factor did not refine to zero. The site occupation factors of ligands and chloride anions were correlated so that the total negative charges were set to −12, to balance the positive charge coming from the $[Zr_6O_4(OH)_4]^{12+}$ metallic node. For the sake of simplicity, the smeared electronic density within the cavities was modelled by DMF molecules alone. The two crystallographically independent DMF molecules were located using a Monte Carlo/Simulated Annealing approach,[15] implemented in TOPAS-R V3. During the final structure refinement stages carried out with the Rietveld method ligand and DMF bond distances (except for the C-H and C=O bonds) were refined in limited ranges of values,[16] retrieved carrying out a search in the Cambridge Structural Database (v. 2020.1) for room-temperature crystal structures containing the 2,2′-biselenophene, 2-carboxyselenophene, 2,2′-

bithiophene-5,5′-dicarboxylate or 2,2′-bithiazole fragments. The background was modelled through a polynomial function of the Chebyshev-type. An isotropic thermal factor [$B_{iso}(M)$] was refined for the Zr^{IV} metal centre; the isotropic thermal factor of lighter atoms belonging to the cluster and the ligands was calculated as $B_{iso}(L) = B_{iso}(M) + 2.0$ ($Å^2$); the isotropic thermal factor of the DMF atoms was calculated as $B_{iso}(S) = B_{iso}(M) + 3.0$ ($Å^2$). The peak profile was modelled trough the Fundamental Parameters Approach.[17] The final Rietveld refinement plots are shown in Figures S7-S10 of the Supporting Information.

Crystal data for **1·S**: cubic, $Pn\overline{3}$, $a = 25.7020(6)$ Å, $V = 16979(1)$ $Å^3$, $Z = 24$, $Z' = 4$, $\rho = 0.991$ g cm^{-3}, $F(000) = 4555.0$, $R_{Bragg} = 0.011$, $R_p = 0.020$ and $R_{wp} = 0.028$, for 4986 data and 73 parameters in the 5.3-105.0° (2θ) range. CCDC No. 2020561

Crystal data for **2·S**: cubic, $Pn\overline{3}$, $a = 25.546(1)$ Å, $V = 16671(3)$ $Å^3$, $Z = 24$, $Z' = 4$, $\rho = 1.005$ g cm^{-3}, $F(000) = 4925.1$, $R_{Bragg} = 0.015$, $R_p = 0.025$ and $R_{wp} = 0.032$, for 4991 data and 86 parameters in the 5.2-105.0° (2θ) range. CCDC No. 2020562.

Crystal data for **3·S**: cubic, $Pn\overline{3}$, $a = 25.564(1)$ Å, $V = 16511(2)$ $Å^3$, $Z = 24$, $Z' = 4$, $\rho = 1.002$ g cm^{-3}, $F(000) = 4874.4$, $R_{Bragg} = 0.015$, $R_p = 0.020$ and $R_{wp} = 0.026$, for 4981 data and 80 parameters in the 5.4-105.0° (2θ) range. CCDC No. 2020563.

Crystal data for **4·S**: cubic, $Pn\overline{3}$, $a = 25.416(2)$ Å, $V = 16417(4)$ $Å^3$, $Z = 24$, $Z' = 4$, $\rho = 1.031$ g cm^{-3}, $F(000) = 5022.6$, $R_{Bragg} = 0.005$, $R_p = 0.019$ and $R_{wp} = 0.024$, for 4991 data and 79 parameters in the 5.2-105.0° (2θ) range. CCDC No. 2020564.

Variable-temperature powder X-ray diffraction. As a representative example, the thermal behaviour of **1·S** was investigated *in situ* by variable-temperature powder X-ray diffraction. A powdered sample (~20 mg) of this MOF was deposited on an aluminium sample-holder and

heated using a custom-made sample heater (Officina Elettrotecnica di Tenno, Ponte Arche, Italy) in the temperature range 303-663 K with steps of 20 K. PXRD patterns were acquired in isothermal conditions in the 2θ range 5.0-25.0°, with steps of 0.02° and a time per step of 1 s, and treated performing a parametric whole powder pattern refinement with the Le Bail method, as implemented in TOPAS-R V3.

Gas Adsorption. Samples of **1·S-4·S** (∼40 mg) were activated at 403 K under high vacuum (10^{-6} Torr) for 24 h before each measurement. The textural properties were estimated by volumetric adsorption carried out with an ASAP 2020 Micromeritics instrument, using N_2 as adsorbate at 77 K. For the Brunauer−Emmett−Teller (BET) specific surface area calculation, the 0.01-0.1 p/p^0 pressure range of the isotherm was used to fit the data. Within this range, all the Rouquerol consistency criteria are satisfied.[18] The pore size distribution was determined on the basis of the NLDFT method (Tarazona model for cylindrical pores).

Luminescence measurements. The experiments were carried out on solids or air-equilibrated DMF suspensions at 298 K unless otherwise noted. UV-vis absorption spectra were recorded with a PerkinElmer λ40 spectrophotometer using quartz cells with path length of 1.0 cm. Luminescence spectra were collected with a PerkinElmer LS-50 or an Edinburgh FLS920 spectrofluorimeter equipped with a Hamamatsu R928 phototube. For solid samples, the emission quantum yield was calculated from corrected emission spectra registered by an Edinburgh FLS920 spectrofluorimeter equipped with a barium sulfate coated integrating sphere (4 in.), a 450W Xe lamp (λ excitation tunable by a monochromator supplied with the instrument) as light source, and a R928 photomultiplier tube, following the procedure described by de Mello *et al*.[19] The estimated experimental errors are 2 nm on the band maximum, 5% on the molar absorption coefficient, and 20% on the emission quantum yield in the solids.

Results and Discussion

Synthesis and crystal structure of H$_2$SpSp and of the related MOFs 1-4. The ditopic linker 2,2'-biselenophene-5,5'-dicarboxylic acid was straightforwardly prepared from ethyl selenophene-2-carboxylate following a literature procedure found for its thiophene analogue[9] *via* Pd^{II}/Ag^{I}-catalyzed homocoupling in DMSO. After chromatographic purification, diethyl 2,2'-biselenophene-5,5'-dicarboxylate (**Et$_2$SpSp**, Scheme S1) was finally converted into the corresponding diacid **H$_2$SpSp** (Scheme 1) in almost quantitative yield (80%) through a basic hydrolysis (NaOH) in water/methanol mixtures followed by acidification of the concentrated aqueous solution of the corresponding sodium dicarboxylate salt (Scheme S1). This synthetic path was preferred to an alternative methodology successfully exploited for the synthesis of the thiophene analogue **H$_2$ThTh**,[6] *i.e.* 2,2′-biselenophene direct carboxylation (treatment of 2,2′-biselenophene with two equivalents of ^{n}BuLi at 195 K followed by CO$_2$ bubbling in the reaction mixture and acidification), because of the much higher product yields. Despite the numerous attempts made, it was not possible to grow single crystals of **H$_2$SpSp** suitable for X-ray diffraction; on the other hand, slow evaporation of ethyl acetate concentrated solutions of the diester **Et$_2$SpSp** led to the formation of bright yellow platelets that were successfully characterized *via* single-crystal X-ray diffraction. The structural details of **Et$_2$SpSp** are collected in the Supporting Information (Table S1 and Figure S1). It crystallizes in the triclinic $P\overline{1}$ space group, with half of a molecule, residing on an inversion center, in the asymmetric unit. Consequently, the two selenium atoms lie on the opposite sides of the exocyclic C–C bond (Se-C-C-Se dihedral angle = 180°). This heteroatom reciprocal *trans* arrangement in conjugated bicyclic compounds is somehow expected as it is the lowest energy conformation. As such, it is also typical of 2,2′-biselenophene,[20] 2,2′-bithiazole,[21] 2,2′-bithiophene[22] and other bicyclic dicarboxylic acids/esters like **H$_2$TzTz**[4] and Hex$_2$ThTh (Hex = *n*-hexyl).[23]

Starting from our optimized synthesis of the thiazole MOF [Zr$_6$O$_4$(OH)$_4$(TzTz)$_6$],[4] reaction of **H$_2$SpSp** with ZrCl$_4$ in *N,N*-dimethylformamide (DMF) under solvothermal conditions and using

concentrated HCl as crystal modulator led to formation of a microcrystalline yellow powder of formula $[Zr_6O_4(OH)_4(SpSp)_{3.8}Cl_{4.4}]\cdot4(DMF)\cdot8(H_2O)$ (**1·S**). The application of the synthetic protocol described above to mixtures of the different (but isostructural) ligands **H₂SpSp**, **H₂ThTh** and **H₂TzTz** (Scheme 1) allowed for the preparation of the pure phase MIXMOFs **2·S-4·S**. The initial linkers relative stoichiometric ratio for the syntheses was set to 3:3 for the double-mixed samples and to 2:2:2 for the triple-mixed MOF. Curiously, in the synthesis of the triple-mixed MOF **4·S** the employment of zirconium oxychloride octahydrate $(ZrOCl_2\cdot8H_2O)$ instead of simple $ZrCl_4$ as metal source was of fundamental importance to get a highly crystalline product ($ZrCl_4$ only gives amorphous phases under the same experimental conditions). The presence of the different heterocyclic spacers within the solid samples is confirmed by the presence of multiple carboxylate stretching bands $[\nu(COO^-)]$ in their IR spectra (see the Experimental Section and Figure S2). According to a well-established experimental methodology already applied to other MIXMOFs from the literature,[24] the actual linkers composition in the as-synthesized materials was assessed *via* ¹H NMR signal integration of the digested samples in acidic solutions (D_2SO_4 in D_2O/DMSO-d_6 mixtures), referring to the diagnostic signals of **H₂SpSp**, **H₂ThTh** and **H₂TzTz** falling in the $7.0 < \delta_H < 9.0$ ppm range (Figures S11-S13). This spectroscopic information has been exploited for the refinement of the crystal structures (see the Experimental Section and below). The samples are pure unique phases and not mixtures of the single-linker MOF components, as witnessed by the DSC traces recorded on **2·S-4·S** (*vide infra*) and by the comparison of the PXRD profiles of a specific MIXMOF and of its single-linker counterparts. As a representative example, the comparison of the powder patterns of the selenophene-thiazole MIXMOF **3·S** and its pure linker parent analogues **1·S** and $[Zr_6O_4(OH)_4(TzTz)_6]\cdot n(DMF)$[4] is shown in Figure S14. As expected, the main diffraction peaks in **3·S** are unique and fall in between those of its parent materials.

1·S-4·S are isostructural with the bithiophene[6] and bithiazole[4] MOFs with general formula $[Zr_6O_4(OH)_4(L)_6]\cdot n(DMF)$. Hence, in here their crystal structure will be jointly described and illustrated by **1·S** as a representative example. For the representation of the crystal structure of **2·S-**

4·S, the reader is addressed to Figures S15-S17 of the Supporting Information. For the sake of simplicity, the discussion is made assuming a perfect crystal without missing ligands and chloride anions. **1·S** crystallizes in the cubic space group $Pn\overline{3}$ and features $Zr_6O_4(OH)_4$ clusters as secondary building units (Figure 1A). The Zr^{IV} metal centres are eight-coordinated, in a square-antiprismatic coordination geometry, by eight oxygen atoms, four coming from the carboxylate groups, which define one square face of the antiprism, and four belonging to μ_3-O and μ_3-OH groups, defining the other square face. The main Zr–O bond distances between the Zr^{IV} ion and the carboxylate oxygen atoms are 2.16 Å (**1·S**), 2.17 Å (**2·S**), 2.15 Å (**3·S**), 2.19 Å (**4·S**). These values are slightly shorter if compared to those of $[Zr_6O_4(OH)_4(ThTh)_6]\cdot n(DMF)$[6] and $[Zr_6O_4(OH)_4(TzTz)_6]\cdot n(DMF)$[4] (2.23 and 2.22 Å, respectively), proving the existence of a stronger coordinative bond. Each $[Zr_6]$ secondary building unit is surrounded by twelve carboxylate groups belonging to twelve different ditopic ligands, forming a 3D open framework (Figure 1B) of **fcu** topology (assigned with the TOPOS 4.0 software,[25] considering the $[Zr_6]$ units as nodes and the ligands as connectors). The structure features octahedral (~11 Å diameter) (Figure 1C) and tetrahedral (~8 Å diameter) (Figure 1D) cages,[26] occupied by solvent molecules. Each octahedral cage is edge-sharing and face-sharing with eight octahedral and eight tetrahedral cavities, respectively. Two crystallographically distinct DMF solvent molecules were located within the octahedral and tetrahedral cavities, respectively. Neglecting the clathrated solvent, the empty unit cell volume of the four MOFs was estimated with the software PLATON[27] in the range 63-65%, in agreement with the values found in $[Zr_6O_4(OH)_4(ThTh)_6]\cdot n(DMF)$[6] and $[Zr_6O_4(OH)_4(TzTz)_6]\cdot n(DMF)$[4] (61 and 62%, respectively); these values translate into pore volumes of about 0.88 cm^3 g^{-1} (**1·S**), 0.87 cm^3 g^{-1} (**2·S**), 0.99 cm^3 g^{-1} (**3·S**), 0.83 cm^3 g^{-1} (**4·S**). All ligands show a *trans* disposition of their heteroatoms on the two heterocyclic rings as that found in their uncoordinated form (see also Figure S1 in the Supporting Information).[21-22, 28] Linker deviation from planarity (with dihedral angles between the two heterocyclic rings falling in the 6-25° range) is observed in all cases, as already found for other structurally characterized coordination compounds from the literature containing the $ThTh^{2-}$ ligand.[29]
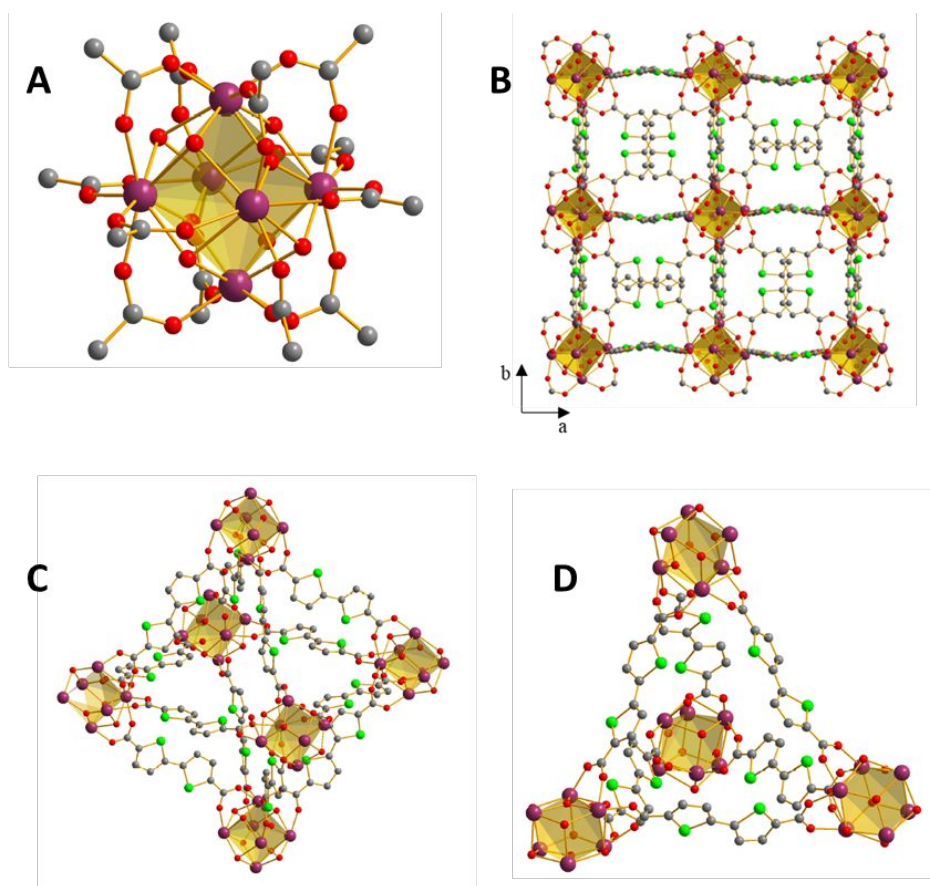
Figure 1. Representation of the crystal structure of **1·S**: (A) the Zr-oxo cluster; (B) portion of the crystal packing viewed along the [100] crystallographic direction; (C) the octahedral cage; (D) the tetrahedral cage. The solvent molecules and hydrogen atoms are omitted. For the sake of simplicity, the graphical model has been built assuming a perfect crystal without missing ligand defects. Atom colour code: carbon, grey; oxygen, red; selenium, light green; zirconium, violet.

Thermal behavior. The thermal analyses (TGA and DSC) carried out under N_2 indicated that **1·S-4·S** undergo the same sequence of events, namely: i) loss of chlatrated solvent; ii) decomposition (Figures S18-S21). The temperature ranges of these events are reported in Table 2.

Table 2. Details of the thermal behaviour of compounds **1·S-4·S**, as observed by TGA under N_2 flow.

		1·S	**2·S**	**3·S**	**4·S**
Loss of solvent	T range (K)	313-473	313-480	313-550	313-600
	Obs. wt. (%)	17.8	16.5	15.7	20.0
	Calc. wt. (%)	16.9	16.3	14.2	22.4
Decomposition	T_{dec} (K)	692	697	676	692
	Res. Mass (%)	24.6	25.0	27.1	29.3
	Chemical residue	$5(ZrC) \cdot ZrO_2$	$6(ZrC)$	$6(ZrC)$	$5(ZrO_2) \cdot ZrS_2$
	(Calc. wt.%)	(24.7)	(25.2)	(26.8)	(29.6)

The decomposition temperature is in the range 675-700 K. The introduction of a bithiophene linker strengthens the structure stability with respect to the pure biselenophene sample (**2** *vs.* **1**), while the opposite occurs with bithiazole (**3** *vs.* **1**). In the triple-mixed MOF **4**, the two effects mutually vanish, and the decomposition temperature equals that of **1**. In addition, the pure biselenophene MOF **1** has a decomposition temperature slightly higher than those of its pure bithiophene $[Zr_6O_4(OH)_4(ThTh)_6]$ (T_{dec} = 663 K)[6] or bithiazole $[Zr_6O_4(OH)_4(TzTz)_6]$ (T_{dec} = 673 K)[4] analogues. This can be related to the different acidity of the corresponding carboxylic acids and their ability at engaging into coordination bonds of variable strength with zirconium. Selenium has a higher polarizability and charge delocalization ability than sulphur, because of its low-energy-lying empty *4d* orbitals. Consequently, selenophene carboxylate is slightly more basic than thiophene carboxylate (pK*a* of the corresponding acids 10.4 and 10.5, respectively).[8] Judging from the residual mass values found, the solid residues at the end of the decomposition process are likely to be simple binary zirconium inorganic compounds like zirconium carbide (ZrC), zirconium oxide (ZrO_2), zirconium sulphide (ZrS_2) or their mixtures; tentative compositions are provided in Table 2. Worthy of note, the existence of a single peak in the DSC curves concomitant with the decomposition of **2·S-4·S** indicates the presence of a unique phase rather than a solid solution. The variable-temperature PXRD experiment carried out on **1·S** as a representative example (Figure S22A) highlighted that the MOF gradually loses its crystallinity starting from room temperature, becoming practically amorphous at 663 K. In the temperature range 303-423 K, the unit cell volume increment is about 0.4% (Figure S22B); this low value reveals the high rigidity of the crystal structure when the external stimulus is the temperature variation.

N₂ adsorption. The four MOFs texture and porosity were evaluated through N_2 adsorption isotherms measured at 77 K. All samples were previously evacuated with a thermal treatment by heating them at 303 K under high vacuum for 24 h, to remove the solvent inside the pores

coming from the synthesis. As shown in Figure 2A, **1-4** show type I isotherms, typical of a microporous material, with BET areas in the $300 \div 550$ m^2/g range. These values are much lower than those found for the pure linker analogues $[Zr_6O_4(OH)_4(ThTh)_6]$ (2207 m^2/g)[6] or $[Zr_6O_4(OH)_4(TzTz)_6]$ (840 m^2/g),[4] possibly because of the defective nature of the samples or due to the rapid loss of crystallinity upon heating (see above). The limiting micropore volume estimated through the application of the Dubinin-Astakhov model to the N$_2$ adsorption isotherm of the real samples equals 0.23, 0.15, 0.12 and 0.19 cm^3/g for **1-4**, respectively. The total pore volumes evaluated at p/p* = 0.98 equal 0.26, 0.23, 0.17 and 0.21 cm^3/g for **1-4**, respectively. In all samples, there are two different micropore sizes (retrieved from the NLDFT analysis – Tarazona model for cylindrical pores) of *ca.* 18 and 22 Å (Figure 2B), in line with the crystallographic results related to the Zr···Zr distances between opposite metallic nodes in the framework and similar to those found for the biphenyl parent MOF UiO-67 (12 and 16 Å).[5]
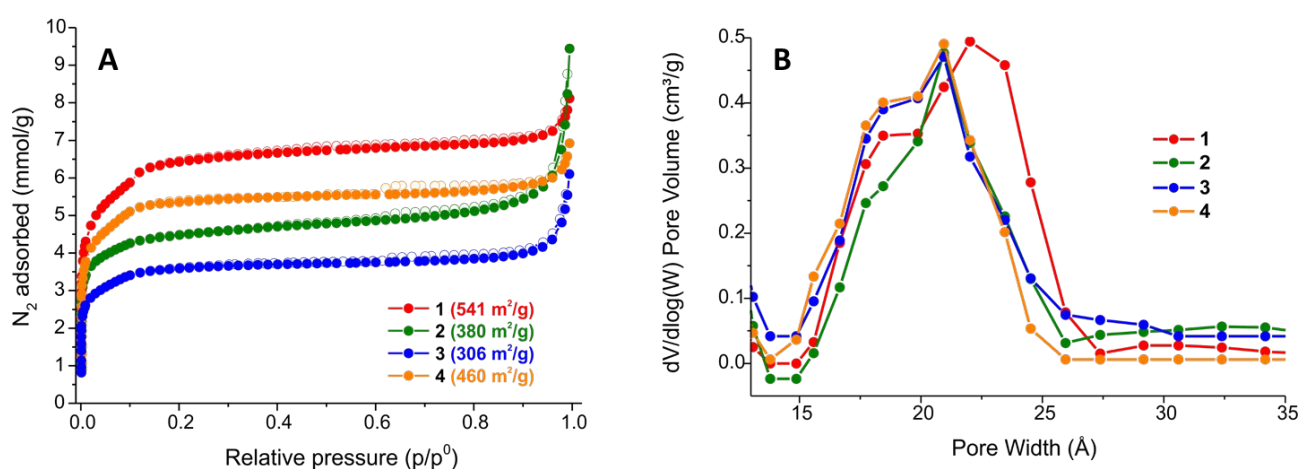

Figure 2. (A) N$_2$ isotherms measured at 77 K on **1-4**. The desorption isotherm branch is depicted with empty symbols. (B) Pore size distribution (NLDFT – Tarazona model for cylindrical pores) of **1-4**.

Luminescence studies. Initially, the luminescent properties of the bare linkers were studied both in DMF solution and in the solid state. In DMF (Figure 3A), the three absorption and emission maxima of **H$_2$SpSp**, **H$_2$ThTh** and **H$_2$TzTz** are found in the $345 < \lambda_{max,abs} < 366$ nm and $405 < \lambda_{max,em} < 435$ nm ranges for absorption and emission, respectively. In the solid state, their emissions are red-

shifted and generate characteristic blue/green colors under a UV lamp, whose CIE chromatic
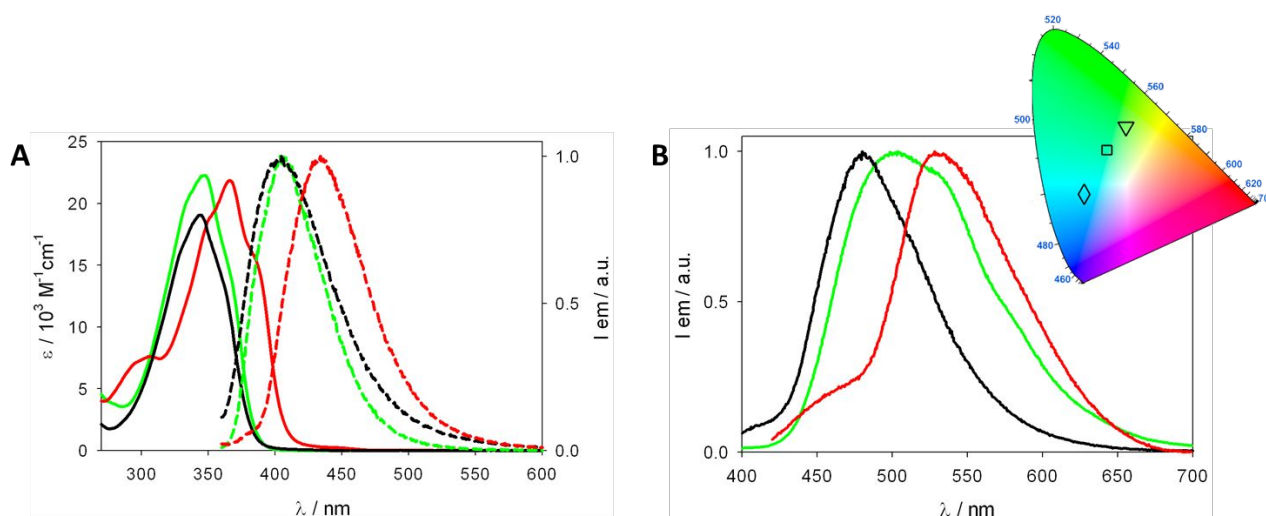
coordinates are shown in Figure 3B.

Figure 3. (A) Absorption (solid lines) and normalized emission spectra (dashed lines) of **H₂SpSp** (red), **H₂ThTh** (green) and **H₂TzTz** (black) in DMF solution at r.t. (λ_{ex}=340 nm). (B) Normalized emission spectra of the same compounds as powders at r.t. (λ_{ex}=390, 350 and 360 nm, respectively). Inset: collective CIE diagram derived from the emission spectra (**H₂SpSp**, triangle; **H₂ThTh**, square; **H₂TzTz**, diamond).

The emission spectra and the CIE diagrams of the related MOFs **1·S-4·S** in DMF suspensions are

reported in Figure 4. The emission maximum of the pure selenophene MOF **1·S** falls at $\lambda = 510$ nm

and it is red-shifted with respect to that of free **H₂SpSp** in DMF; this shift may be caused by the

chromophore coordination to Zr^{IV}. In the MIXMOF samples, the emission wavelengths ($\lambda_{max} = 485$,

450 and 485 nm for **2·S-4·S**, respectively) are associated to blue-green colors. More specifically, the

biselenophene/bithiazole MOF **3·S** shows CIE coordinates in the blue region, while the other

compounds are closer to green. Blue emitters show applications in displays and solid-state lighting,[30]

while green-colored LEDs are exploited in medical fields (chromotherapy). Green light helps to

lighten hyper-pigmentation spots and has calming and anti-inflammatory properties. In addition, the

green color is slightly sedative with beneficial effects for sleep and stress reduction.[31] Unfortunately,

the emission intensity is rather low, falling under the ordinary detection limit set for solid-state

materials (luminescence quantum yield < 0.05 found in all samples). This phenomenon is frequently

observed in the crystalline solid state, where organic-based multicolor emission is hampered by

fluorophores aggregation, phase separation and mutual quenching.[32] This problem was also

encountered in other literature MOFs where all the organic linkers in the framework are emissive
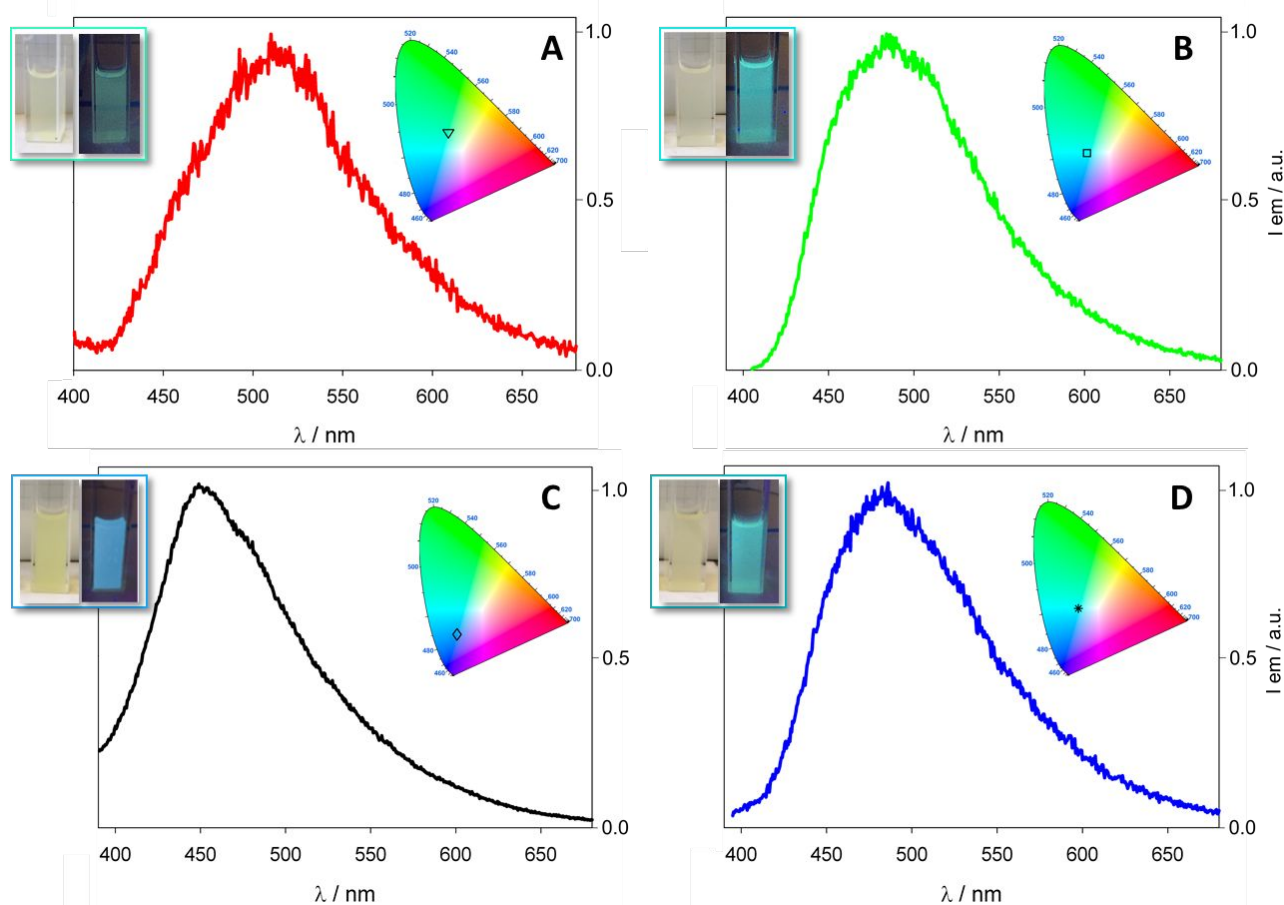
fluorophores.[33]

Figure 4. Normalized emission spectra and corresponding CIE diagrams of **1·S-4·S** in DMF suspension. Inset: photos taken on the suspensions under ambient light (left) and under UV excitation (right). A: **1·S**; B:**2·S**; C: **3·S**; D: **4·S**. 360 < λ_{ex} < 380 nm.

Conclusions

Four novel microporous (MIX)MOFs with five-membered S/Se-containing heterocyclic linkers

bound to zirconium nodes have been prepared and fully characterized in the solid state. Selenophene,

thiophene and thiazole are luminescent organic molecules that find application in the fields of

LEDs and optoelectronics. Their inclusion into an ordered crystalline scaffold kept together

by [Zr$_6$] secondary building units produces luminescent materials emitting in the blue-green

visible range upon excitation by a suitable UV wavelength. The measured emission quantum

yields are low in all cases, because of self-quenching effects coming from the formation of non-fluorescent aggregates in the solid state. This is a proof of evidence that the crystal lattice is made of domains containing the same linker type instead of being distributed randomly within the solid matrix. When chemically different linkers form large clusters within the lattice, the fluorescence is completely quenched, as recently shown in a seminal work published by Zhou and co-workers.[34] A viable strategy to solve this problem is the "solid state dilution" of the chromophore using an excess of another non-emissive spacer for the MIXMOF construction.[35] This approach is currently being pursued in our laboratories for the preparation of MIXMOFs featured by enhanced luminescence properties.

Conflicts of Interest. The authors have no conflicts of interest to declare.

Associated Content

Supporting Information. Main crystallographic data, experimental details and structure refinement details for **Et₂SpSp**, IR spectra of **1·S-4·S** at comparison, XRF spectra of **1·S-4·S**, graphical results of the structure refinement for **1·S-4·S**, ¹H NMR spectra of the digested mixed samples **2·S-4·S** in D_2SO_4, representation of the crystal structures of **2·S-4·S**, additional PXRD information, TGA-DTG-DSC plots for **1·S-4·S**, VT-PXRD experiment on **1·S**.

Author Information

Corresponding Author

* Dr. Andrea Rossin. E-mail: a.rossin@iccom.cnr.it

* Prof. Simona Galli. E-mail: simona.galli@uninsubria.it

* Dr. Andrea Fermi. E-mail: andrea.fermi2@unibo.it

ORCID

Andrea Rossin: 0000-0002-1283-2803

Simona Galli: 0000-0003-0335-5707

Marco Moroni: 0000-0001-6167-3792

Giuliano Giambastiani: 0000-0002-0315-3286

Andrea Fermi: 0000-0003-1080-0530

Giacomo Bergamini: 0000-0002-2135-4073

References

1. (a) Ghosh, S. Eds., *Metal-Organic Frameworks (MOFs) for Environmental Applications*. Elsevier (Amsterdam): 2019 (b) García, H.; Navalón, S. Eds., *Metal‐Organic Frameworks: Applications in Separations and Catalysis*. Wiley-VCH: 2018 (c) Rossin, A.; Tuci, G.; Luconi, L.; Giambastiani, G., Metal–Organic Frameworks as Heterogeneous Catalysts in Hydrogen Production from Lightweight Inorganic Hydrides. *ACS Catal.* **2017,** *7*, 5035–5045 (d) Moghadam, P. Z.; Li, A.; Wiggin, S. B.; Tao, A.; Maloney, A. G. P.; Wood, P. A.; Ward, S. C.; Fairen-Jimenez, D., Development of a Cambridge Structural Database Subset: A Collection of Metal−Organic Frameworks for Past, Present, and Future. *Chem. Mater.* **2017,** *29*, 2618-2625 (e) Kaskel, S. Eds., *The Chemistry of Metal-Organic Frameworks: Synthesis, Characterization, and Applications*. Wiley-VCH: 2016 (f) Seyyedi, B., Eds., *Metal-Organic Frameworks: a New Class of Crystalline*

Porous Materials. Lambert Academic Publishing: Saarbrücken: 2014 (g) MacGillivray, L. R.; Lukehart, C. M., Eds., *Metal-Organic Framework Materials*. John Wiley & Sons: New York: 2014 (h) Suh, M. P.; Park, H. J.; Prasad, T. K.; Lim, D. W., Hydrogen Storage in Metal–Organic Frameworks. *Chem. Rev.* **2012,** *112*, 782-835 (i) Farrusseng, D., Eds., *Metal-Organic Frameworks: Applications from Catalysis to Gas Storage*. Wiley-VCH Verlag: Weinheim: 2011 (j) Schroeder, M., Eds., *Functional Metal-organic Frameworks: Gas Storage, Separation and Catalysis*. Springer-Verlag: Berlin, Heidelberg: 2010 (k) Horcajada, P.; Serre, C.; Maurin, G.; Ramsahye, N. A.; Balas, F.; Vallet-Regi, M.; Sebban, M.; Taulelle, F.; Férey, G., Flexible Porous Metal-Organic Frameworks for a Controlled Drug Delivery. *J. Am. Chem. Soc.* **2008,** *130*, 6774–6780.

2. (a) Ding, B.; Hua, C.; Kepert, C. J.; D'Alessandro, D. M., Influence of Structure–Activity Relationships on Through-Space Intervalence Charge Transfer in Metal–Organic Frameworks with Cofacial Redox-Active Units. *Chem. Sci.* **2019,** *10*, 1392-1400 (b) Hua, C.; D'Alessandro, D. M., Systematic Tuning of Zn(II) Frameworks with Furan, Thiophene, and Selenophene Dipyridyl and Dicarboxylate Ligands. *Cryst. Growth Des.* **2017,** *17*, 6262-6272.

3. (a) Alghamdi, A. A. B.; Watters, D. C.; Yi, H.; Al-Faifi, S.; Almeataq, M. S.; Coles, D.; Kingsley, J.; Lidzey, D. G.; Iraqi, A., Selenophene *vs.* Thiophene in Benzothiadiazole-Based Low Energy Gap Donor–Acceptor Polymers for Photovoltaic Applications. *J. Mater. Chem. A* **2013,** *1*, 5165-5171 (b) Haid, S.; Mishra, A.; Uhrich, C.; Pfeiffer, M.; Bauerle, P., Dicyanovinylene-Substituted Selenophene-Thiophene Co-oligomers for Small-Molecule Organic Solar Cells. *Chem. Mater.* **2011,** *23*, 4435-4444 (c) Heeney, M.; Zhang, W.; Crouch, D. J.; Chabinyc, M. L.; Gordeyev, S.; Hamilton, R.; Higgins, S. J.; McCulloch, I.; Skabara, P. J.; Sparrowe, D.; Tierney, S., Regioregular Poly(3-Hexyl)Selenophene: a Low Band Gap Organic Hole Transporting Polymer. *Chem. Commun.* **2007**, 5061-5063.

4. Müller, P.; Bucior, B.; Tuci, G.; Luconi, L.; Getzschmann, J.; Kaskel, S.; Snurr, R. Q.; Giambastiani, G.; Rossin, A., Computational Screening, Synthesis and Testing of Metal–Organic

Frameworks with a Bithiazole Linker for Carbon Dioxide Capture and its Green Conversion into Cyclic Carbonates. *Mol. Syst. Des. Eng.* **2019,** *4*, 1000-1013.

5. Cavka, J. H.; Jakobsen, S.; Olsbye, U.; Guillou, N.; Lamberti, C.; Bordiga, S.; Lillerud, K. P., A New Zirconium Inorganic Building Brick Forming Metal Organic Frameworks with Exceptional Stability. *J. Am. Chem. Soc.* **2008,** *130*, 13850-13851.

6. Yoon, M.; Moon, D., New Zr (IV) Based Metal-Organic Framework Comprising a Sulfur-Containing Ligand: Enhancement of CO_2 and H_2 Storage Capacity. *Microp. Mesop. Mater.* **2015,** *215*, 116-122.

7. (a) Luo, T.-Y.; Liu, C.; Gan, X. Y.; Muldoon, P. F.; Diemler, N. A.; Millstone, J. E.; Rosi, N. L., Multivariate Stratified Metal–Organic Frameworks: Diversification Using Domain Building Blocks. *J. Am. Chem. Soc.* **2019,** *141*, 2161–2168 (b) Zhang, X.; Frey, B. L.; Chen, Y.-S.; Zhang, J., Topology-Guided Stepwise Insertion of Three Secondary Linkers in Zirconium Metal–Organic Frameworks. *J. Am. Chem. Soc.* **2018,** *140*, 7710-7715 (c) Pang, J.; Yuan, S.; Qin, J.; Wu, M.; Lollar, C. T.; Li, J.; Huang, N.; Li, B.; Zhang, P.; Zhou, H.-C., Enhancing Pore-Environment Complexity Using a Trapezoidal Linker: Toward Stepwise Assembly of Multivariate Quinary Metal−Organic Frameworks. *J. Am. Chem. Soc.* **2018,** *140*, 12328-12332 (d) Feng, L.; Yuan, S.; Li, J.-L.; Wang, K.-Y.; Day, G. S.; Zhang, P.; Wang, Y.; Zhou, H.-C., Uncovering Two Principles of Multivariate Hierarchical Metal−Organic Framework Synthesis via Retrosynthetic Design. *ACS Cent. Sci.* **2018,** *4*, 1719-1726 (e) Feng, L.; Yuan, S.; Zhang, L.-L.; Tan, K.; Li, J.-L.; Kirchon, A.; Liu, L.-M.; Zhang, P.; Han, Y.; Chabal, Y. J.; Zhou, H.-C., Creating Hierarchical Pores by Controlled Linker Thermolysis in Multivariate Metal−Organic Frameworks. *J. Am. Chem. Soc.* **2018,** *140*, 2363-2372 (f) Sun, Y.; Sun, L.; Feng, D.; Zhou, H.-C., An In Situ One-Pot Synthetic Approach towards Multivariate Zirconium MOFs. *Angew. Chem. Int. Ed.* **2016,** *55*, 6471-6475 (g) Yuan, S.; Lu, W.; Chen, Y.-P.; Zhang, Q.; Liu, T.-F.; Feng, D.; Wang, X.; Qin, J.; Zhou, H.-C., Sequential Linker Installation: Precise Placement of Functional Groups in Multivariate Metal−Organic Frameworks. *J. Am. Chem. Soc.* **2015,** *137*, 3177-3180 (h) Burrows, A. D., Mixed-

Component Metal–Organic Frameworks (MC-MOFs): Enhancing Functionality through Solid Solution Formation and Surface Modifications. *CrystEngComm* **2011,** *13*, 3623-3642.

8. Arcoria, A.; Maccarone, E.; Mamo, A., Nucleophilic Substitution in the Side Chain of Five-membered Heterocycles. Part 4. Reaction Kinetics of Selenophene Compounds. *J. Chem. Soc., Perkin Trans. 2* **1979**, 1347-1352.

9. Masui, K.; Ikegami, H.; Mori, A., Palladium-Catalyzed C-H Homocoupling of Thiophenes: Facile Construction of Bithiophene Structure. *J. Am. Chem. Soc.* **2004,** *126*, 5074-5075.

10 The accurate solvent content has been assessed through TG-DTG analysis on the bulk sample.

11. Katz, M. J.; Brown, Z. J.; Colón, Y. J.; Siu, P. W.; Scheidt, K. A.; Snurr, R. Q.; Hupp, J. T.; Farha, O. K., A Facile Synthesis of UiO-66, UiO-67 and their Derivatives. *Chem. Commun.* **2013**, 9449-9451

12. *Topas, V. 3.0*; Bruker AXS: Karlsruhe, Germany, **2005**.

13. Bond distances and angles for the rigid body describing: (a) the ligands: C2-C3/N3 and C4-C5, 1.38 Å; C3/N3-C4, 1.42 Å; C-Se, 1.88 Å; C-S, 1.72 Å; C-C and C=O of the carboxylic functionalization, 1.48 and 1.25 Å, respectively; C-H, 0.95 Å; C-C exocyclic bond, 1.54 Å; rings internal bond angles, C-C-C and C-C-Se, 113.2°; C-C-S, 112.5°; C-C-H external bond angles, 123.4 Å; (b) the DMF molecule: C=O, 1.25 Å; C-N, 1.35 Å; C-H, 0.95 Å; bond angles for sp^2 and sp^3 atoms, 120° and 109.5°, respectively.

14. (a) Øien, S.; Wragg, D.; Reinsch, H.; Svelle, S.; Bordiga, S.; Lamberti, C.; Lillerud, K. P., Detailed Structure Analysis of Atomic Positions and Defects in Zirconium Metal–Organic Frameworks. *Cryst. Growth Des.* **2014,** *14*, 5370-5372 (b) Valenzano, L.; Civalleri, B.; Chavan, S.; Bordiga, S.; Nilsen, M. H.; Jakobsen, S.; Lillerud, K. P.; Lamberti, C., Disclosing the Complex Structure of UiO-66 Metal Organic Framework: A Synergic Combination of Experiment and Theory. *Chem. Mater.* **2011,** *23*, 1700-1718.

15. Coelho, A. A., Whole-Profile Structure Solution from Powder Diffraction using Simulated Annealing. *J. Appl. Crystallogr.* **2000,** *33*, 899-908.

16. C2-C3/N3 and C4-C5, 1.36-1.42 Å; C3/N3-C4, 1.37-1.45 Å; C-Se bond, 1.84-1.91 Å; C-S bond, 1.68-1.84 Å; C-C of the carboxylic functionalization, 1.45-1.55 Å; C-C exocyclic bond, 1.40-1.55 Å; C-N bonds in the DMF molecule, 1.35-1.45 Å.

17. Cheary, R. W.; Coelho, A. A., A Fundamental Parameters Approach to X-Ray Line-Profile Fitting. *J. Appl. Cryst.* **1992,** *25*, 109-121.

18. (a) Gómez-Gualdrón, D. A.; Moghadam, P. Z.; Hupp, J. T.; Farha, O. K.; Snurr, R. Q., Application of Consistency Criteria To Calculate BET Areas of Micro-And Mesoporous Metal−Organic Frameworks. *J. Am. Chem. Soc.* **2016,** *138*, 215-224 (b) Rouquerol, J.; Llewellyn, P.; Rouquerol, F., In *Studies in Surface Science and Catalysis*, Llewellyn, P. L.; Rodriquez-Reinoso, F.; Rouquerol, J.; Seaton, N., Eds. Elsevier Amsterdam, 2007; Vol. 160, p 49.

19. de Mello, J. C.; Wittmann, H. F.; Friend, R. H., An Improved Experimental Determination of External Photoluminescence Quantum Efficiency. *Adv. Mater.* **1997,** *9*, 230-232.

20. Inoue, S.; Jigami, T.; Nozoe, H.; Aso, Y.; Ogura, F.; Otsubo, T., Syntheses, Spectroscopic Properties and Polymerizations of 2,2'-Bitellurophene, 2,2':5',2"-Tertellurophene and Related Hybrid Terchalcogenophenes. *Heterocycles* **2000,** *52*, 159-170.

21. Craig, D. C.; Goodwin, H. A.; Onggo, D.; Rae, A. D., Coordination of 2,2'-Bithiazole. Spectral, Magnetic and Structural Studies of the Iron(II) and Nickel(II) Complexes. *Aust. J. Chem.* **1988,** *41*, 1625-1644.

22. Pelletier, M.; Brisse, F., Bithiophene at 133 K. *Acta Crystallogr. Sect. C* **1994,** *C50*, 1942-1945.

23. Wang, S.; Brisse, F., Alternating Conjugated and Nonconjugated Polymer. 1. Crystal Structures and Polymorphism of Poly(hexamethylene 2,2'-bithiophene-5,5'-dicarboxylate), P6BT. *Macromolecules* **1998,** *31*, 2265-2277.

24. (a) Luconi, L.; Mercuri, G.; Islamoglu, T.; Fermi, A.; Bergamini, G.; Giambastiani, G.; Rossin, A., Benzothiazolium-Functionalized NU-1000: a Versatile Material for Carbon Dioxide Adsorption and Cyanide Luminescence Sensing. *J. Mater. Chem. C* **2020,** *8*, 7492-7500 (b) Islamoglu, T.; Goswami, S.; Li, Z.; Howarth, A. J.; Farha, O. K.; Hupp, J. T., Postsynthetic Tuning

of Metal−Organic Frameworks for Targeted Applications. *Acc. Chem. Res.* **2017,** *50*, 805-813 (c) Deria, P.; Bury, W.; Hupp, J. T.; Farha, O. K., Versatile Functionalization of the NU-1000 Platform by Solvent-Assisted Ligand Incorporation. *Chem. Commun.* **2014,** *50*, 1965-1968 (d) Cohen, S. M., Postsynthetic Methods for the Functionalization of Metal–Organic Frameworks. *Chem. Rev.* **2012,** *112*, 970-1000 (e) Tanabe, K. K.; Cohen, S. M., Postsynthetic Modification of Metal–Organic Frameworks - a Progress Report. *Chem. Soc. Rev.* **2011,** *40*, 498-519.

25. Blatov, V. A.; Shevchenko, A. P.; Proserpio, D. M., Applied Topological Analysis of Crystal Structures with the Program Package ToposPro. *Cryst. Growth Des.* **2014,** *14*, 3576-3586. http://topospro.com/

26. The cages diameter was estimated by measuring the distance among the nearest carbon atoms of ligands belonging to opposite cage walls and subracting the Van der Waals radii of the two atoms.

27. Spek, A. L., Structure Validation in Chemical Crystallography. *Acta Crystallogr. Sect. D* **2009,** *65*, 148–155.

28. Lukevics, E.; Arsenyan, P.; Belyakov, S.; Pudova, O., Molecular Structure of Selenophenes and Tellurophenes. (Review). *Chem. Heterocycl. Compd.* **2002,** *38*, 763-777.

29. (a) Earl, L. D.; Patrick, B. O.; Wolf, M. O., Synthesis, Structure, and Magnetic Properties of Bithiophene- and Terthiophene-Linked Manganese Metal−Organic Frameworks. *Inorg. Chem.* **2013,** *52*, 10021-10030 (b) Jankolovits, J.; Lim, C.-S.; Mezei, G.; Kampf, J. W.; Pecoraro, V. L., Influencing the Size and Anion Selectivity of Dimeric Ln^{3+}[15-Metallacrown-5] Compartments through Systematic Variation of the Host Side Chains and Central Metal. *Inorg. Chem.* **2012,** *51*, 4527-4538 (c) Earl, L. D.; Patrick, B. O.; Wolf, M. O., Synthesis, Structure, and Luminescent Properties of Oligothiophene-Containing Metal–Organic Frameworks. *CrystEngComm* **2012,** *14*, 5801-5808.

30. (a) Lee, J.; Chen, H.-F.; Batagoda, T.; Coburn, C.; Djurovich, P. I.; Thompson, M. E.; Forrest, S. R., Deep Blue Phosphorescent Organic Light-Emitting Diodes with Very High Brightness and Efficiency. *Nat. Mater.* **2016,** *15*, 92-98 (b) Holmes, R. J.; Forrest, S. R.; Sajoto, T.; Tamayo, A.;

Djurovich, P. I.; Thompson, M. E.; Brooks, J.; Tung, Y. J.; D'Andrade, B. W.; Weaver, M. S.; Kwong, R. C.; Brown, J. J., Saturated Deep Blue Organic Electrophosphorescence Using a Fluorine-Free Emitter. *Appl. Phys. Lett.* **2005,** *87*, 243507.

31. (a) Minguillon, J.; Lopez-Gordo, M. A.; Renedo-Criado, D. A.; Sanchez-Carrion, M. J.; Pelayo, F., Blue Lighting Accelerates Post-Stress Relaxation: Results of a Preliminary Study. *PLoS ONE* **2017,** *12*, e0186399 (b) Al-Ayash, A.; Kane, R. T.; Smith, D.; Green-Armytage, P., The Influence of Color on Student Emotion, Heart Rate, and Performance in Learning Environments. *Color Res. Appl.* **2015,** *41*, 196-205.

32. (a) Kaeser, A.; Schenning, A. P. H. J., Fluorescent Nanoparticles Based on Self-Assembled π-Conjugated Systems. *Adv. Mater.* **2010,** *22*, 2985-2997 (b) Ryu, J.-H.; Hong, D.-J.; Lee, M., Aqueous Self-Assembly of Aromatic Rod Building Blocks. *Chem. Commun.* **2008,** *9*, 1043-1054.

33. Cornelio, J.; Zhou, T.-Y.; Alkaş, A.; Telfer, S. G., Systematic Tuning of the Luminescence Output of Multicomponent Metal−Organic Frameworks. *J. Am. Chem. Soc.* **2018,** *140*, 15470-15476.

34. Li, J.; Yuan, S.; Qin, J.-S.; Huang, L.; Bose, R.; Pang, J.; Zhang, P.; Xiao, Z.; Tan, K.; Malko, A. V.; Cagin, T.; Zhou, H.-C., Fluorescence Enhancement in the Solid State by Isolating Perylene Fluorophores in Metal−Organic Frameworks. *ACS Appl. Mater. Interfaces* **2020,** *12*, 26727-26732.

35. Newsome, W. J.; Ayad, S.; Cordova, J.; Reinheimer, E. W.; Campiglia, A. D.; Harper, J. K.; Hanson, K.; Uribe-Romo, F. J., Solid State Multicolor Emission in Substitutional Solid Solutions of Metal−Organic Frameworks. *J. Am. Chem. Soc.* **2019,** *141*, 11298-11303.

1
2
3
4
5
6
7
8
9
10
11
12
13
14
15
16
17
18
19
20
21
22
23
24
25
26
27
28
29
30
31
32
33
34
35
36
37
38
39
40
41
42
43
44
45
46
47
48
49
50
51
52
53
54
55
56
57
58
59
60

TOC Graphic